J Therm Anal Calorim (2014) 115:1057–1063
DOI 10.1007/s10973-013-3427-2

Temperature dependence of thermal diffusivity, specific heat capacity, and thermal conductivity for several types of rocks

S. Q. Miao · H. P. Li · G. Chen

Received: 6 September 2013 / Accepted: 18 September 2013 / Published online: 8 October 2013

Abstract The thermo-physical properties for four rock types (granite, granodiorite, gabbro, and garnet amphibolite) from room temperature to 1,173 K were investigated. Thermal diffusivity and specific heat capacity were measured using the laser-flash technique and heat flux differential scanning calorimetry, respectively. Combined with the density data, rock thermal conductivities were calculated. Rock thermal diffusivity and conductivity decrease as the temperature increases and approach a constant value at high temperatures. At room temperature, the measured thermal conductivity is consistently near or lower than the calculated conductivity using the mineral series model, which suggests that real thermal conduction is more complicated than is depicted in the model. Therefore, in situ measurement remains the best method for accurately obtaining thermal conductivity for rocks.

Keywords Thermal diffusivity · Specific heat capacity · Thermal conductivity · High temperatures · Rock · Laser-flash technique

Introduction

Mineral and rock thermo-physical properties are important geological parameters and indispensable factors for retrieving Earth's evolutionary history. Crustal rock thermal conductivity (e.g., for granite, limestone, basalt, and granulite) is key to calculating the local surface heat flux, whereas thermal conductivity for mantle rocks (e.g., lherzolite, ferropericlase, and silicate perovskite) is essential to comprehend thermal regimes in the mantle and their evolution with time [1, 2].

Geological material thermal conductivities were first measured in 1940 [3], and over the past half century, measurement methods and accuracy have greatly improved. Currently, measurements can be performed under not only high temperatures but also high pressures [4–6].

Material thermal conductivities depend not only on temperature but also pressure. For most geological materials, thermal conductivity decreases to 40–60 % of the original value when the temperature increases from room temperature to 1,273 K. When the pressure increases by 1 GPa, the thermal conductivity increases by approximately 4 % of ambient pressure value [7]. For crustal rocks, the maximum temperature could be 1,073 K, and the pressure is below 1.5 GPa [8]. Therefore, the pressure effect on thermal conductivity can be neglected. Thermal conductivity measured under high temperatures and normal pressure represents the real thermal conductivity under crustal conditions.

Compared with the few methods for thermal conductivity measurements at high temperatures and high pressures, more methods are available for measurements under normal pressure and high temperatures conditions. Among such methods, the laser-flash technique is preferred [9]; it is a non-contact method that avoids the inevitable thermal contact resistance for traditional contact methods. Moreover, graphite and silver film coating on the sample surface can prohibit direct radiative transfer. Therefore, the real lattice thermal conductivity for samples can be derived. This method directly measures thermal diffusivity for

S. Q. Miao · H. P. Li (✉) · G. Chen
Laboratory for High Temperature and High Pressure Study of the Earth's Interior, Institute of Geochemistry, Chinese Academy of Sciences, Guiyang 550002, China
e-mail: lihp0803@163.com

S. Q. Miao · G. Chen
University of Chinese Academy of Sciences, Beijing 100049, China

samples and calculates thermal conductivity through the sample specific heat capacity and density. Because sample thickness is the only parameter involved, this method is highly precise, with a 3 % nominal error [4].

Detailed studies have been performed for certain common minerals (e.g., quartz, feldspar, pyroxene, olivine, and garnet) using this method, and the temperature dependence of the thermal diffusivity for such minerals was discerned [10–14]. Whittington [15] discerned thermal diffusivity for granite and rhyolite at a high temperature using the laser-flash technique. More recently, basalt, granulite, greenstone, tonalite–trondhjemite–granodiorite, dolomite, and rhyolite glasses have been measured using the laser-flash technique [16–19]. In this study, we measured thermal diffusivity for granite, granodiorite, gabbro, and garnet amphibolite from room temperature to 1,173 K using the laser-flash technique. In addition, we measured the specific heat capacity at high temperatures using heat flux differential scanning calorimetry. The sample thermal conductivities were calculated as:

$$k = D \times C_P \times \rho \quad (1)$$

where k was thermal conductivity; D was thermal diffusivity; C_P was heat capacity at constant pressure [20]. The rock samples herein were collected from the North China craton, and thus the results can provide constraints for petrology studies in the North China craton area.

Experimental work

Sample preparation

The investigated samples in our work were obtained from different regions of the North China craton. The mineralogical composition was determined using thin sections and point-counting technique under a polarizing microscope. Density and porosity were measured using the Micro-ultraPYC 1200e true density analyzer [21]. The summary of the description of the samples were summarized on Table 1. The major elements were determined on air-dry crushed and milled samples using the X-ray fluorescence (XRF) method from pressed pellets. The results were given in Table 2.

The bulk samples were cut into disks by means of an impregnated diamond-slitting disk. After slitting, the sample faces was polished and lapped parallel. The samples were prepared in the shape of disks with 12.70 mm diameter and 2.50 mm thickness to be suitable for the thermal diffusivity measurement. The upper and lower disk surfaces were coated with graphite and silver film. This process inhibits direct radiative transfer at high temperatures and promotes laser heat absorption at the lower surface. The graphite–silver coating was 20-μm thick; thus, it did not affect the measurement results. Powder samples were prepared for specific heat capacity measurement.

Table 1 Summary of the description of the samples

Sample	Color	Texture, fabric	Grain size	Mineralogical composition	Sample site	Density/ g cm^{-3}	Porosity/ %
Granite	Light gray	Granitic texture, Isotropic	Coarse	Oligoclase (70 %), quartz (25 %), biotite (3 %), magnetite (1 %), microcline (1 %)	Fuping, Hebei	2.620	3.20
Granodiorite	Light gray	Granular texture, Isotropic	Coarse	Andesine (68 %), biotite (10 %), hornblende (10 %), quartz (10 %), magnetite (1 %), potassium feldspar (1 %)	Fangshan, Beijing	2.674	2.60
Gabbro	Dark gray	Gabbro texture, Isotropic	Coarse	Labradorite (60 %), clinopyroxene (40 %)	Liangcheng, Inner Mongolia	2.969	0.93
Garnet amphibolite	Dark gray	Granular texture, Isotropic	Coarse	Hornblende (60 %), plagioclase (29 %), garnet (10 %), magnetite (1 %)	Fuping, Hebei	2.991	4.08

Table 2 XRF analyses (mass/%) of the samples

Sample	SiO_2	Al_2O_3	FeO_{tot}	MgO	CaO	Na_2O	K_2O	MnO	P_2O_5	TiO_2	L.O.I.	Total
Granite	69.11	15.43	1.65	4.18	2.75	4.39	1.49	–	0.03	0.24	0.42	99.96
Granodiorite	62.04	16.30	5.02	4.18	3.59	3.92	3.41	0.04	0.29	0.62	0.26	100.15
Gabbro	49.73	15.98	11.43	9.39	9.83	1.78	0.73	0.16	0.13	0.74	0.47	100.68
Garnet amphibolite	48.95	14.03	13.25	10.66	8.27	2.07	1.08	0.18	0.29	1.11	0.65	100.80

L.O.I. loss of ignition

Measurements

In this experiment, the laser-flash apparatus (LFA427) was used to measure the sample thermal diffusivity [22, 23]. Figure 1 shows a schematic diagram for the LFA427. The system has three main parts: the laser heating system, high temperature furnace, and temperature detector [4]. The gray disk in the high temperature furnace represents the sample. Measurement began when the sample temperature reached an expected value and was stable. The Nd:GGG solid-state laser produced a pulse with the wavelength 1,064 nm and ms-wide to heat the sample bottom. The maximum energy can reach 25 J. The sample temperature increased after heating, and the upper surface of the sample released heat through radiation. The IR sensor (InSb) at the top of the instrument recorded the heat signal temporal variations. Thermal diffusivity (D) was calculated based on the thermal conduction model equation

$$D = 0.1388 \times l^2/t_{0.5} \quad (2)$$

where l was the sample thickness, and $t_{0.5}$ was the time when the upper surface of the sample reached half of the maximum temperature [9].

After the sample was positioned, the furnace was vacuumed and filled with inert gas. With a 20 K min^{-1} heating rate, measurement began when the temperature reached a particular value and remained stable. During the measurement process, the maximum temperature increase inside the sample associated with the laser pulse was less than 3 °C. Therefore, the thermal diffusivity measured was for the furnace preset temperature [4]. The measurement result for the standard materials before the experiment indicated that the instrument operated properly. The temperature interval was 100 K in the medium range and 200 K in the high temperature range. Each temperature point was measured three times, and the average value was calculated as the final thermal diffusivity.

The specific heat capacity was measured using the STA449C Simultaneous Thermal Analyzer (Netzsch-Gerätebau, Germany) based on heat flux differential scanning calorimetry (DSC) [24, 25]. The resolution of DSC signal was 1.00 μW, and the accuracy of the derived values of specific heat capacity was 0.02 J g^{-1} K^{-1}. The samples were ground because powdered sample ensures good thermal contact with the crucible. 50 mg powder was used for measurement. The reference sample was 15 mg sapphire with a known specific heat capacity, and the container was a $Pt_{90}Rh_{10}$ crucible. The heating rate was 20 K min^{-1}, and the temperature range was 300–1,400 K. The entire process was conducted under an Argon gas flux (40 mL min^{-1}). Using this instrument, we also measured thermo-gravimetry (TG) (at a 25-ng resolution). The combination of DSC and TG data provided a reference for analyzing the dehydration, degasification, and decomposition reactions during heating.

Results and discussion

Thermal diffusivity (D)

The temperature dependence of the thermal diffusivities in the temperature range from room temperature to 1,173 K for the investigated samples was shown in Fig. 2. The thermal diffusivities were fitted to

$$D = a + b/T \quad (3)$$

where a and b are fitting parameters [4]. The fitting parameters were shown in Table 3.

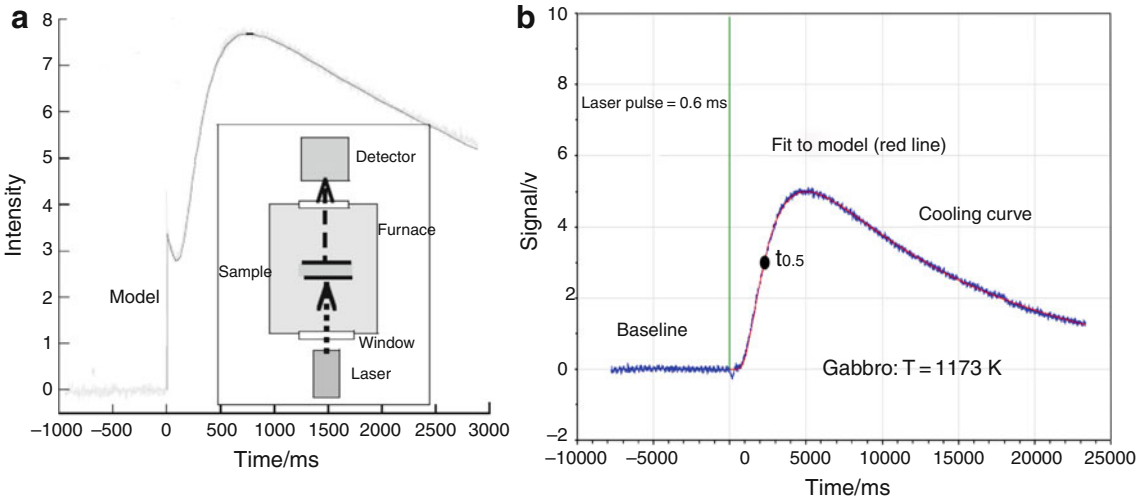

Fig. 1 **a** Schematic diagram for the laser-flash technique (modified after Hofmeister [4]). **b** Raw data of gabbro at 1,173 K

As shown in the Fig. 2, at room temperature, the rocks' thermal diffusivities are in the range 0.8–1.3 $mm^2\ s^{-1}$. As the temperature increases, thermal diffusivity monotonically decreases. Granite decreases more strongly than other rocks. At high temperatures rocks' thermal diffusivities were in the range of 0.4–0.6 $mm^2\ s^{-1}$, and approach constant values, respectively. It is because that thermal diffusivity is connected with the number of phonons within the primitive unit cell. As temperature increases, overtone-combination modes are excited, but saturation in the number of modes occurs when T is high enough that the continuum dominates the statistics, and increasing T no longer significantly changes the number of phonons. The flat trend in D occurs at high temperatures [4]. The granite result is close (slightly lower) to that of felsic mylonitic granite, as measured by Nabelek [16]. At room temperature, all the rocks have relatively higher thermal diffusivity than monzonite because of the weak conducting ability of feldspar [19].

Specific heat capacity (C_P)

Specific heat capacities ($Jg^{-1}\ K^{-1}$) were fitted to [26]

$$C_P = a + bx^{-2} + cx^{-3} + dx^{-0.5} + ex^{-1} \quad (4)$$

The fitting parameters were given in Table 4.

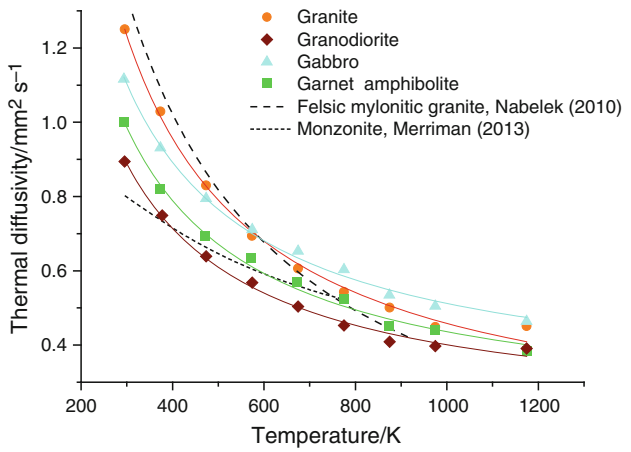

Fig. 2 Temperature dependence of thermal diffusivity for samples

Table 3 Fitting parameters of thermal diffusivity

	a	b	R^2
Granite	0.12620	332.09	0.99503
Granodiorite	0.19208	208.80	0.99390
Gabbro	0.25860	253.37	0.99593
Garnet amphibolite	0.20054	235.43	0.99314

Thermal conductivity (k)

Ignoring the density change associated with thermal expansion, thermal conductivity can be calculated by Eq. (1). The temperature dependence of the thermal conductivity in the temperature range from room temperature to 1,173 K for the investigated samples was shown in Fig. 3. Thermal conductivities were fitted to [27]

$$k = (c + dT)^{-1} \quad (5)$$

where c (thermal resistance at zero temperature) was related to the scattering of phonons by impurities and imperfections, and d (rate of increase in the thermal resistance) was related to phonon–phonon scattering. The fitting parameters were shown in Table 5.

As shown in the Fig. 3, at room temperature, the rocks' thermal conductivities are in the range 1.9–2.6 $W\ m^{-1}\ K^{-1}$. As the temperature increases, thermal conductivity monotonically decreases. Granite contains high content of quartz, which will result in a high value of conductivity at room temperature and a rapid decrease of thermal conductivity with increasing temperature. At room temperature, Gabbro, garnet amphibolite as well as granodiorite have the second largest thermal conductivities. At high temperatures, thermal conductivity also approach constant values with range of 1.26–1.55 $W\ m^{-1}\ K^{-1}$, because the phonons are limited in space with the lattice constant size and the mean free phonon path no longer decreases with increasing temperatures, which limits the value of the rocks at high temperatures. Because the specific heat capacity for rocks increases with temperature, which produces a compensating effect on the decreasing thermal conductivity, the decreasing rate of thermal conductivity is lower than for thermal diffusivity.

For the four datasets, the relationship between c and d can be fitted to a linear fitting with

$$c = -528 \times d + 0.5197, \quad R^2 = 0.452 \quad (6)$$

This result is consistent with a statistical study on thermal conductivity for a large number of rocks by Seipold [27].

Rocks are aggregates of various minerals. Therefore, rock thermal conductivities can theoretically be calculated from the constituent mineral thermal conductivities. However, the mineral grain size and arrangement must be considered. The simplest case assumes that different minerals are connected in parallel or series. Then, in accordance with the theorem for thermal resistance in parallel or series connections, the total thermal conductivity for series connections is

$$k_m = \sum_{i=1}^{n} v_i k_i \quad (7)$$

Table 4 Fitting parameters of specific heat capacity

	Granite	Granodiorite	Gabbro	Garnet amphibolite
a	−0.22824	0.82608	4.8967	2.2989
b	3.3801×10^5	-2.1770×10^5	-1.2089×10^6	0.28035×10^5
c	-3.4738×10^7	3.6131×10^7	1.2317×10^8	3.1541×10^6
d	110.88	17.837	−290.79	−33.204
e	−2378.1	0	6447.4	0
R^2	0.96089	0.99769	0.97677	0.97606

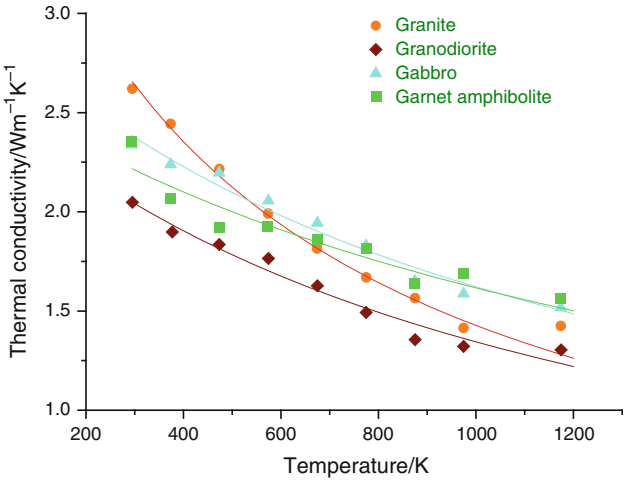

Fig. 3 Temperature dependence of the thermal conductivity for samples

Table 5 Fitting parameters of thermal conductivity

	c	d	R^2
Granite	0.24094	4.6019×10^{-4}	0.99602
Granodiorite	0.41836	3.5002×10^{-4}	0.96353
Gabbro	0.33727	2.7932×10^{-4}	0.96912
Garnet amphibolite	0.38133	2.3740×10^{-4}	0.89204

and the total thermal conductivity for parallel connections is

$$k_m = \left(\sum_{i=1}^{n} \frac{v_i}{k_i} \right)^{-1} \tag{8}$$

where v_i and k_i are the volume fraction and thermal conductivity for the ith material, respectively.

The Maxwell–Eucken model assumes that one or multiple discontinuous phases are evenly distributed in the frame formed by the continuous phases. The EMT model assumes that the constituents are randomly distributed [28]. Suppose the minerals inside the rocks are ordered by these four modes, the rock thermal conductivity can be calculated based on the different minerals thermal conductivities at room temperature. The results were shown in Table 6, and the thermal conductivities at room temperature are: 1.88 for oligoclase [29], 9.37 for quartz [10], 1.83 for biotite [30], 2.91 for hornblende [30], 4.75 for clinopyroxene [13], and 3.56 for garnet [4].

From Table 6, we found that the parallel model has the largest thermal conductivity and the series model has the smallest among the connection models. The Maxwell–Eucken and EMT models have medium values, and the thermal conductivities for the two models are close. At ambient temperature and pressure, measured thermal conductivities are near or lower than the conductivities calculated from the mineral series model, which is similar to the observations by Kukkonen [31] and suggests that real thermal conduction is more complicated than is indicated in a model. The pores, fractures, and grain boundaries may play an important role in this process. Therefore, in situ measurement remains the best method for accurately obtaining thermal conductivity for rocks.

For the surface heat flux calculation, we refer to Fourier's law of thermal conduction:

$$q = k \times \mathrm{d}T/\mathrm{d}z \tag{9}$$

Table 6 Comparison of measured thermal conductivity and calculated thermal conductivity obtained from various models at room temperature

	Parallel/ W m^{-1} K^{-1}	Series/ W m^{-1} K^{-1}	Maxwell–Eucken/ W m^{-1} K^{-1}	EMT/ W m^{-1} K^{-1}	Measured/ W m^{-1} K^{-1}	Porosity/ %
Granite	4.127	2.473	3.044	3.264	2.620	3.20
Granodiorite	2.628	2.117	2.291	2.312	1.917	2.60
Gabbro	3.028	2.479	2.760	2.814	2.347	0.93
Garnet amphibolite	2.666	2.539	2.629	2.627	2.347	4.08

where q is heat flux, dT/dz is temperature gradient. The temperature gradient for sampling points is generated using in situ measurements, while rock thermal conductivities at the sampling point are measured in the lab [1]. The sampling point is typically underground, with an 8 km maximum depth. At that depth, the temperature is in the range 373–573 K [8]. Rock thermal conductivities are only 70 % of room-temperature. Because high levels of data must be processed to produce a statistically average value for thermal conductivity, previous measurements were limited to normal temperature and pressure conditions. Herein, thermal conductivity rapidly decreases at high temperatures. Therefore, thermal conductivity at high temperatures must be used for more accurate surface heat flux data. For example, the garnet amphibolite is the primary type of rock in the mid-crust [32]. According to the surface heat flux and crust shell structure for different blocks in North China craton area, the mid-crust temperature is 573–873 K. Thus, the corresponding thermal conductivity should be in the range 1.7–1.9 W m^{-1} K^{-1}, in contrast to 2.4 W m^{-1} K^{-1} at room temperature.

Conclusions

In this study, we measured thermal diffusivity for four types of rock (granite, granodiorite, gabbro, and garnet amphibolite) from room temperature to 1,173 K using the laser-flash apparatus LFA427. The rocks' specific heat capacities from room temperature to 1,173 K were measured using the simultaneous thermal analyzer STA449C. Combined with the density data, the thermal conductivities from room temperature to 1,173 K were calculated. The results suggest that the method used herein is applicable for accurately determining thermo-physical properties for rocks in the temperature range of Earth's deep interior. When the temperature increases, thermal diffusivity and thermal conductivity decrease. The decreasing thermal conductivity is close to a linear profile. At high temperature, thermal diffusivity and thermal conductivity approach constant values. At room temperature, the measured thermal conductivity is consistently near or lower than the calculated conductivity using the mineral series model, which suggests that real thermal conduction is more complicated than indicated by the model. Therefore, in situ measurement remains the best method for accurately obtaining thermal conductivity for rocks.

The results herein are preliminary. For use in geology models, the samples should include more common rocks.

Acknowledgements The study was performed under Project supported by "135" Program of Chinese Academy of Sciences.

References

1. Sass JH, Lachenbruch AH, Munroe RJ. Thermal conductivity of rocks from measurements on fragments and its application to heat-flow determinations. J Geophys Res. 1971;76(14):3391–401. doi:10.1029/JB076i014p03391.
2. van den Berg AP, Yuen DA. Delayed cooling of the earth's mantle due to variable thermal conductivity and the formation of a low conductivity zone. Earth Planet Sci Lett. 2002;199(3–4):403–13.
3. Birch F, Clark H. The thermal conductivity of rocks and its dependence upon temperature and composition. Am J Sci. 1940;238(9):613–35.
4. Hofmeister AM. Thermal diffusivity of garnets at high temperature. Phys Chem Miner. 2006;33(1):45–62.
5. Ohta K, Yagi T, Taketoshi N, Hirose K, Komabayashi T, Baba T, et al. Lattice thermal conductivity of MgSiO3 perovskite and post-perovskite at the core-mantle boundary. Earth Planet Sci Lett. 2012;349–350:109–15.
6. Pohlmann C, Hutsch T, Röntzsch L, Weißgärber T, Kieback B. Novel approach for thermal diffusivity measurements in inert atmosphere using the flash method. J Therm Anal Calorim. 2013. doi:10.1007/s10973-013-3048-9.
7. Hofmeister AM. Mantle values of thermal conductivity and the geotherm from phonon lifetimes. Science. 1999;283(5408):1699–706.
8. Chapman DS. Thermal gradients in the continental crust. Geol Soc Spec Publ. 1986;24(1):63–70.
9. Parker WJ, Jenkins RJ, Abbott GL, Butler CP. Flash method of determining thermal diffusivity, heat capacity, and thermal conductivity. J Appl Phys. 1961;32(9):1679–84.
10. Branlund JM, Hofmeister AM. Thermal diffusivity of quartz to 1,000 degrees C: effects of impurities and the alpha-beta phase transition. Phys Chem Miner. 2007;34(8):581–95.
11. Pertermann M, Whittington AG, Hofmeister AM, Spera FJ, Zayak J. Transport properties of low-sanidine single-crystals, glasses and melts at high temperature. Contrib Mineral Petrol. 2008;155(6):689–702.
12. Hofmeister A, Whittington A, Pertermann M. Transport properties of high albite crystals, near-endmember feldspar and pyroxene glasses, and their melts to high temperature. Contrib Mineral Petrol. 2009;158(3):381–400.
13. Hofmeister AM, Pertermann M. Thermal diffusivity of clinopyroxenes at elevated temperature. Eur J Mineral. 2008;20(4):537–49.
14. Pertermann M, Hofmeister AM. Thermal diffusivity of olivine-group minerals at high temperature. Am Mineral. 2006;91(11–12):1747–60.
15. Whittington AG, Hofmeister AM, Nabelek PI. Temperature-dependent thermal diffusivity of the earth's crust and implications for magmatism. Nature. 2009;458(7236):319–21.
16. Nabelek PI, Whittington AG, Hofmeister AM. Strain heating as a mechanism for partial melting and ultrahigh temperature metamorphism in convergent orogens: implications of temperature-dependent thermal diffusivity and rheology. J Geophys Res. 2010;115(B12):B12417. doi:10.1029/2010jb007727.
17. Romine W, Whittington A, Nabelek P, Hofmeister A. Thermal diffusivity of rhyolitic glasses and melts: effects of temperature, crystals and dissolved water. Bull Volcanol. 2012;74(10):2273–87.
18. Nabelek PI, Hofmeister AM, Whittington AG. The influence of temperature-dependent thermal diffusivity on the conductive cooling rates of plutons and temperature-time paths in contact aureoles. Earth Planet Sci Lett. 2012;317:157–64.
19. Merriman JD, Whittington AG, Hofmeister AM, Nabelek PI, Benn K. Thermal transport properties of major archean rock types to high temperature and implications for cratonic geotherms. Precambrian Res. 2013;233:358–72.

20. Rutkowski P, Piekarczyk W, Stobierski L, Górny G. Anisotropy of elastic properties and thermal conductivity of Al2O3/h-BN composites. J Therm Anal Calorim. 2013. doi:10.1007/s10973-013-3246-5.
21. Li S, Wang S, Li X, Li Y, Liu S, Coulson IM. A new method for the measurement of meteorite bulk volume via ideal gas pycnometry. J Geophys Res. 2012;117(E10):E10001. doi:10.1029/2012je004202.
22. Cha J, Seo J, Kim S. Building materials thermal conductivity measurement and correlation with heat flow meter, laser flash analysis and TCi. J Therm Anal Calorim. 2012;109(1):295–300.
23. Parameshwaran R, Jayavel R, Kalaiselvam S. Study on thermal properties of organic ester phase-change material embedded with silver nanoparticles. J Therm Anal Calorim. 2013. doi:10.1007/s10973-013-3064-9.
24. Hirono T, Hamada Y. Specific heat capacity and thermal diffusivity and their temperature dependencies in a rock sample from adjacent to the Taiwan Chelungpu fault. J Geophys Res. 2010;115(B5):B05313. doi:10.1029/2009jb006816.
25. Mojumdar SC, Sain M, Prasad RC, Sun L, Venart JES. Selected thermoanalytical methods and their applications from medicine to construction. J Therm Anal Calorim. 2007;90(3):653–62.
26. Saxena SK. Earth mineralogical model: Gibbs free energy minimization computation in the system MgO–FeO–SiO_2. Geochim Cosmochim Acta. 1996;60(13):2379–95.
27. Seipold U. Temperature dependence of thermal transport properties of crystalline rocks—a general law. Tectonophysics. 1998;291(1–4):161–71.
28. Wang J, Carson JK, North MF, Cleland DJ. A new structural model of effective thermal conductivity for heterogeneous materials with co-continuous phases. Int J Heat Mass Transf. 2008;51(9–10):2389–97.
29. Branlund JM, Hofmeister AM. Heat transfer in plagioclase feldspars. Am Mineral. 2012;97(7):1145–54.
30. Clauser C, Huenges E. Thermal conductivity of rocks and minerals. Rock phys phase relat. 1995;3:105–26.
31. Kukkonen IT. Thermal properties of rocks at the investigation sites: measured and calculated thermal conductivity, specific heat capacity and thermal diffusivity. Helsinki, Finland. Geological Survey of Finland. 1998. 9798/97/AJH.
32. Christensen NI, Mooney WD. Seismic velocity structure and composition of the continental crust: a global view. J Geophys Res. 1995;100(B6):9761–88. doi:10.1029/95JB00259.